Joint Calibration of Multiplatform Altimeter Measurements of Wind Speed and Wave Height over the Past 20 Years

S. ZIEGER, J. VINOTH, AND I. R. YOUNG

Faculty of Engineering and Industrial Sciences, Swinburne University of Technology, Hawthorn, Victoria, Australia

(Manuscript received 3 March 2009, in final form 13 July 2009)

ABSTRACT

Since 1985, for a period of more than 23 yr, seven altimeter missions have provided global coverage of significant wave height and wind speed. This study undertakes a long-term analysis of the accuracy and stability of altimeter-derived values of significant wave height and wind speed from the following satellites: *European Remote Sensing-1* (*ERS-1*), *ERS-2*, *Environmental Satellite* (*Envisat*), *Geosat, Geosat Follow-On* (*GFO*), *Jason-1*, and the Ocean Topography Experiment (TOPEX). This study is a necessary step in developing a quality-controlled and fully calibrated and validated dataset from the combined satellites. Calibration of all altimeters is performed against National Oceanographic Data Center (NODC) buoy data over the extended period. These calibrations are validated using intercomparisons between satellite missions at crossover ground points. This analysis shows that, for a number of the satellites, small "step like" changes occur during the missions. These inconsistencies are removed by subdividing these missions and undertaking a partial calibration for each section of the mission. The analysis also highlights that care is necessary when attempting to apply relationships between radar cross section and wind speed derived for one altimeter to other platforms. Before undertaking such steps, it is first necessary to apply a platform-specific radar cross-sectional offset to the data.

1. Introduction

Many oceanographic applications require the compilation of long-term databases of accurate oceanic properties (in the present case, significant wave height H_s and wind speed U_{10}). Historically, such wave climate data are gathered through the deployment of oceanographic buoys and more recently though the use of numerical models (Caires et al. 2004). Both approaches have significant deficiencies. In situ buoy data have obvious limitations in terms of geographical and temporal coverage and the expense of deploying and maintaining such systems. Model data clearly solve these limitations but rely critically on the accuracy of the model. Even though present-day models contain sophisticated representations of wind–wave physics, the accuracy of such models is still limited (Tolman 2002). Studies by, for example, Dobson et al. (1987) and Monaldo (1988) have shown that active remote sensing satellites, particularly

Ku-band radar altimeter systems, are capable of measuring significant wave height H_s and wind speed U_{10} to an accuracy comparable to in situ observations (e.g., buoys).

Since the launch of *Geosat* in 1985, a total of seven independent altimeter missions (cf. Fig. 2b) have been operational, potentially providing a unique database with global coverage spanning more than two decades. Once calibrated and quality controlled, such a database could be an invaluable tool for many oceanographic applications, such as

- measurement of changes in global wind and wave climate;
- development of methods to determinate extreme values; and
- investigation of extreme meteorological systems (i.e., hurricanes).

To date, however, these independent data sources have not been compiled to form one single, long-term database. Although some attempts have been made to form datasets from combined altimeter missions (e.g., Cotton and Carter 1994; Callahan et al. 1994; Young 1999a; Alves and Young 2003), a comprehensive database of the type proposed has not previously been developed.

Corresponding author address: S. Zieger, Swinburne University of Technology, Faculty of Engineering and Industrial Sciences, P.O. Box 218 (H38), Hawthorn, VIC 3122, Australia.
E-mail: szieger@swin.edu.au

Furthermore, procedures to process data gathered by polar-orbiting altimeter satellites are still relatively underdeveloped. The future of oceanography will inextricably move toward satellite observations of the ocean, supported by in situ point instruments for data calibration.

This paper describes the development of such a database, including the validation, calibration, and quality control of the dataset. The arrangement of the paper is as follows: section 2 describes both the buoy and altimeter data sources used. Section 3 provides details of the quality control and calibration/validation of the altimeter data. Calibrated results for wind speed and wave height are given within the subsections. Finally, the conclusions of the study are considered in section 4, which provides a tabular summary of the final calibrated results for wind speed and wave height.

2. Data sources

National Oceanographic Data Center (NODC) buoy data were used to provide in situ data for a uniform calibration (''ground truthing'') for all altimeter missions over the entire period (described later). The satellite data [geophysical data records (GDRs)] were sourced from the respective agencies and separately compiled for each available radar altimeter up to 2008, covering the historic satellite platforms *Geosat*, *European Remote Sensing-1* (*ERS-1*), and the Ocean Topography Experiment (TOPEX) and the ongoing missions *Environmental Satellite* (*Envisat*), *ERS-2*, *Geosat Follow-On* (*GFO*), and *Jason-1*. Note that the TOPEX/Poseidon mission included three separate altimeter instruments: TOPEX side A (cycles 1–235), TOPEX side B (cycles 236–481), and the Poseidon altimeter. The Poseidon altimeter has not been considered in this paper because its data are coincident with TOPEX.

a. Buoy data

Wind and wave data were downloaded from the National Oceanic and Atmospheric Administration (NOAA) Marine Environmental Buoy Database, which is maintained by the NODC. The data archive contains records from various stations (e.g., lighthouses, oil platforms, buoys, etc.) reporting a range of environmental parameters (e.g., air temperature, sea temperature, wind speed, wave height, wave direction, etc.) in constant time intervals (Evans et al. 2003). Despite the lack of spatial coverage, this archive features an excellent temporal coverage back to the early seventies. For the present purposes, only moored buoys were processed.

The buoy data format (F291) contains nine different types of data records (e.g., nondirectional wave spectra, subsurface temperature/salinity, subsurface current, etc.).
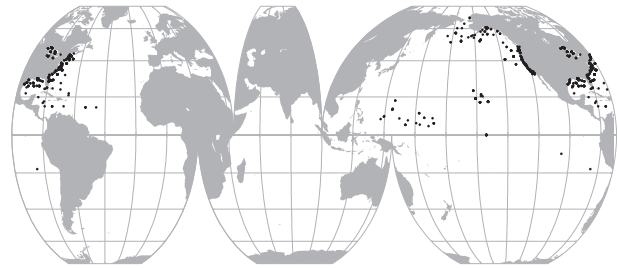

FIG. 1. Global distribution of all 195 NODC buoy stations distributed over 619 different locations based on a Mollweide interrupted equal-area projection. The spatial coverage is clearly limited to the Northern Hemisphere, and the temporal coverage features hourly records since 1985.

In the present analysis, only header and environmental data records were processed (NODC 2008). In addition to geographic location and date–time, values of significant wave height, wind speed, air–sea temperature, and anemometer height were extracted from the environmental data records. The NODC moored buoy network consists of various platform types ranging from 3-, 6-, 10-, to 12-m discus buoys (Meindl and Hamilton 1992). Large discus buoys were deployed in areas of harsh climate, such as the Bering Sea; because of maintenance services and refurbishing procedures, all buoys are subjected to changes in their location with time (Meindl and Hamilton 1992). For calibration purposes, the database consists of 195 different stations distributed over 619 locations. The locations of the buoys are shown in Fig. 1, highlighting the restricted geographical distribution of data, with the vast majority of the locations being near continental North America and almost exclusively confined to the Northern Hemisphere.

Each buoy type collects wind speed at a different height (anemometer height). Therefore, a height-based correction was applied to provide compatibility between buoy observations and altimeter-estimated wind speeds at 10 m (U_{10}) above the mean sea surface. Following Young (1999b) and assuming a logarithmic marine boundary layer, the records were corrected to 10-m reference height U_{10} using the relationship

$$U_{10} = u \sqrt{\frac{\kappa^2}{C_d}} \ln^{-1}\left(\frac{z}{z_o}\right), \qquad (1)$$

where u is the wind speed measured at a height z above sea level, z_o is the surface roughness length, κ is the von Kármán constant, and C_d is the drag coefficient. The drag coefficient varies with both wind speed and sea state (Young 1999b). However, field measurements of C_d typically scatter over an order of magnitude. Noting this and the inherent inaccuracies associated with floating buoy measurements of wind speed (see later this section),

a constant value of C_d was used. For the present application, a representative value of $C_d = 1.5 \times 10^{-3}$ was adopted; with the von Kármán constant $\kappa = 0.4$, (5.11) from Young (1999b) can be solved to yield $z_o = 3.271 \times 10^{-4}$ m. This value of z_o is consistent with the relationship developed by Donelan (1990): $z_o/H_{rms} = 5.53 \times 10^{-4}(U_{10}/C_p)^{2.66}$, where C_p is the phase speed of the waves and H_{rms} is the root-mean-square (rms) wave height. Typical open ocean values of $U_{10}/C_p \approx 1$ and $H_{rms} \approx 0.8$ m yield results comparable to $z_o = 3.271 \times 10^{-4}$ m.

The buoy network transmits hourly observations via the Geostationary Operational Environmental Satellite (GOES) system to the data acquisition center (Hamilton 1986). Some care needs to be exercised in interpreting the logging cycles for the buoys, which have changed over the extended period being considered. Typically, the buoys record wind speed averaged over a period of 8 min and the significant wave height from a time series of duration 20 min. Occasionally, however, the significant wave height was determined from a 40-min time series. The 20-min wave records typically commence 20 min past the hour, and the wind records typically commence 42 min past the hour. On a small number of occasions, the wave records commenced 30 min past the hour (i.e., both wind and wave records conclude at 50 min past the hour). When 40-min wave records were employed, these records commenced on the hour. Records recorded after 5 May 1992 typically recorded the observation time as 50 min past the hour (i.e., the time when wind and wave records concluded). Prior to this date, the recording time was stored as the closest whole hour (i.e., the next hour for records concluding at 50 min past the hour; NODC 2008, personal communication). For the present analysis, the times associated with wind and wave records were corrected to the center of the respective time series.

In the present analysis, buoy data are used as the reference or "ground truth." However, such data are not free of error, because they are limited by both sampling variability (i.e., the respective time series are just one realization of the process; Bendat and Piersol 1971) and instrumental accuracy. Floating buoys are subject to systematic bias. At low wind speeds, the rocking motion of the buoy will "pump" the anemometer, resulting in an overestimation of wind speed. Conversely, at high wind speed/wave height, sheltering by wave crests will result in an underestimation of the wind speed. Buoy accuracies are specified as 1.0 m s^{-1} for wind speed and 0.2 m for significant wave height (NDBC 2008).

b. Altimeter data

Spaceborne radar altimeters have observed the oceans for more than two decades. Figure 2 shows the various
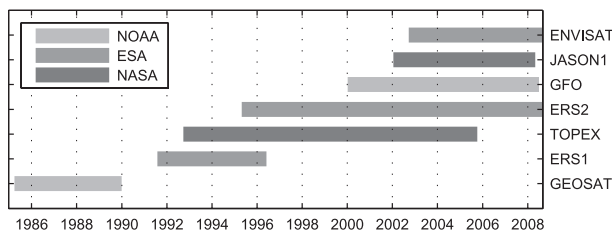

FIG. 2. Temporal coverage of available datasets of the previous seven altimeter missions.

missions over this period. As can be seen, there is an almost continuous record since 1985. The radar altimeter can be used to estimate several oceanographic parameters over a footprint ranging between 1 and 10 km in diameter (Chelton et al. 2001). The precise size of a pulse-limited footprint depends on range, pulse width, and wave height itself (Chelton et al. 2001). The footprint for *Geosat* is approximately 5 km (Cheney et al. 1987); *ERS-1*, *ERS-2*, and *Envisat* are 7 km; TOPEX and *Jason-1* are 6 km (Queffeulou 2004); and *GFO* is approximately 3 km (Walker 1995).

The altimeter estimates significant wave height H_s from the sea surface variance σ^2, which is characterized by the slope of the leading edge of the returned waveform (Chelton et al. 2001; Holthuijsen 2007). The significant wave height is defined as $H_s = 4\sqrt{\sigma^2}$, where σ^2 is the variance of the sea surface elevation (Chelton et al. 2001). Wind speed U_{10} is related to the backscatter coefficient σ_o representing the ratio of the power scattered back to the altimeter from the illuminated surface to the incident power (Chelton et al. 2001). For small incident angles, the radar cross section σ_o can be inversely related to the surface wind speed (Brown et al. 1981, hereafter BR81; Goldhirsh and Dobson 1985, hereafter GD85; Chelton and Wentz 1986, hereafter CW86; Witter and Chelton 1991, hereafter WC91; Young 1993; Freilich and Challenor 1994, hereafter FC94; Young and Holland 1996; Chelton et al. 2001; Abdalla 2007, hereafter A07). Typically, altimeter measurements of H_s have smaller error than for U_{10} when compared with buoy measurements, and the accuracy [rms error (rmse)] has been stated as within 0.5 m for H_s and 1.8–2.0 m s^{-1} for U_{10}. For TOPEX altimeter measurements, Kshatriya et al. (2001) state smaller values of 0.3 m and 1.6 m s^{-1}, respectively.

Data for each of the seven satellites were obtained as detailed in Table 1. The details of the orbit geometry (i.e., repeat cycle and inclination angle) are different for each satellite. However, all systems were placed in polar orbits providing global coverage, with the period of data available shown in Fig. 2. As indicated in Table 1, in each case, GDRs have been used for the analysis. This is

TABLE 1. Summary of altimeter data products and characteristics, including orbit parameters, name of data format, and data source.

Satellite	Dates	Repeat cycle	Inclination	Agency	Format	Source
ERS-1	1 Aug–10 Dec 1991	3 days	98.54°	ESA	CEOS	CD-ROM
	28 Dec 1991–30 Mar 1992	3 days		ESA	CEOS	
	14 Apr 1992–20 Dec 1993	35 days		ESA	CCSDS	
	23 Dec 1993–10 Apr 1994	3 days		ESA	CEOS	
	10 Apr–26 Sep 1994	168 days		ESA	CEOS	
	28 Sep 1994–21 Mar 1995	168 days		ESA	CEOS	
	21 Mar 1995–17 May 1996	35 days		ESA	CCSD	
ERS-2	21 Apr 1995–8 Sep 2008	35 days	98.54°	ESA	CCSD	CD-ROM
Envisat	24 Sep 2002–17 Nov 2008	35 days	98.54°	ESA	RA-2/MWR Level 2	CD-ROM
Geosat	30 Mar 1985–1 Jan 1990	17 days	108.00°	NOAA	JGM3-GDR	CD-ROM
GFO	7 Jan 2000–1 Jul 2008	17 days	108.04°	NOAA	GDR	Internet
Jason-1	15 Jan 2002–03 May 2008	10 days	66.04°	NASA	PODAAC IGDR and GDR	Internet
TOPEX	22 Sep 1992–08 Oct 2005	10 days	66.04°	NASA	PODAAC MGDR-B	Internet

important, because calibration values and data quality often vary between different altimeter data products.

3. Quality control and validation/calibration methods

a. Altimeter quality control

GDRs are not free from errors, and a visual examination of such data clearly shows data "spikes" (see Fig. 3). Such erroneous data often occur at the land–sea boundary, in the proximity of islands, or over sea ice. In compiling a large database, it is important that such erroneous data are removed in a reliable fashion while not discarding reliable data. In a similar fashion to that proposed by Young and Holland (1996), a three-pass quality-control process was applied to the data.

1) PASS 1

The GDRs contain data that enable an initial quality assessment. The first pass focused on the H_s data and flagged data that met any of the following criteria as erroneous:

- If $H_s > 30$ m, then the data point was flagged as erroneous.
- Most datasets contain a flag that indicates whether the data point is over ocean or land/ice, based on a land/sea mask. All points identified as over land/ice were flagged as erroneous.
- GDRs typically provide an observation approximately once per second. Each 1-s value is the average of between 10 and 20 waveforms, depending on the satellite. Waveforms that do not meet predefined parameters are discarded. If the final number of waveforms averaged falls significantly below the maximum possible (10 or 20), then this is an indication that the data are of questionable quality. The number of waveforms averaged for each point is typically recorded within the

GDR. If the number of averaged waveforms was less than 75% of the maximum number, the data were flagged as erroneous.

2) PASS 2

The data from pass 1 were divided into blocks of 25 points. Such blocks represent approximately 180 km along the ground track. This distance was considered large enough to obtain a representative group of observations (25 in this case) but not so long that there would be significant variability within the block resulting from geophysical processes (e.g., different wind systems, etc.). A number of different block sizes were tested before adopting this value.

- Individual values in the block were flagged as erroneous if $|H_s - \overline{H}_s(\text{block})|/\sigma_{H_s}(\text{block}) > 2$, where $\overline{H}_s(\text{block})$ is the mean of the points in the block and $\sigma_{H_s}(\text{block})$ is the standard deviation of the block.

3) PASS 3

In the final pass, blocks identified in pass 2 were further considered. These blocks were redivided into subblocks, either side of flagged points. These subblocks were further considered.

- Each subblock was examined for outliers, as in pass 2, with any further points failing the test flagged as erroneous.
- If the ratio $R = \sigma_{H_s}(\text{block})/\overline{H}_s(\text{block})$ is large, then it indicates that it is possible that there are multiple spikes in the block. Therefore, if $R > 0.5$, then the entire subblock was discarded.

Figure 3 shows an example of a typical satellite pass, with the raw GDR data (gray) and the quality-controlled data (solid lines) shown as well. The ascending ground track is shown as a smooth line (Fig. 3, left) with recorded wave
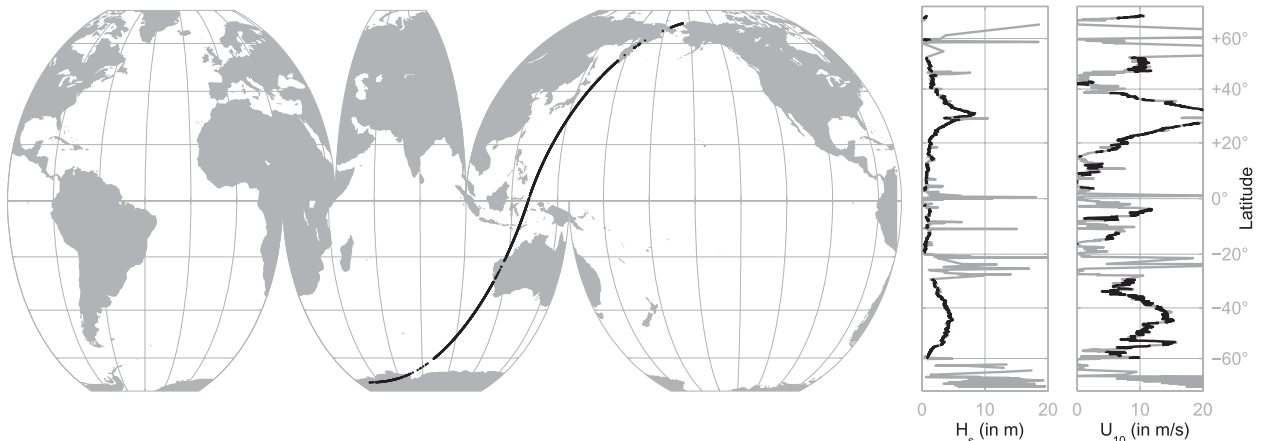
FIG. 3. (left) Ascending *GFO* ground track recorded on 5 Sep 2007 (cycle 201, pass 34) commencing over Antarctica and proceeding over the Southern Ocean and North Pacific Ocean toward the Arctic Ocean. (right) The terms H_s and U_{10} as a function of latitude recorded along the ground track. Data errors (spikes) are clearly evident in the data. This erroneous data (shown in gray) have been removed by the quality-control process.

height H_s and wind speed U_{10} along the ground track as a function of latitude (Fig. 3, right). The most southern section of the track passes over the Antarctic continent toward the Southern Ocean. Because of the Southern Hemisphere winter, erroneous data below 60°S can be linked to sea ice. At approximately 30°S, data spikes occur because of the transition from water to the Australian continent, whereas the effects of islands are shown between 20°S and 10°N when the satellite passes over Indonesia. Farther north, valid data are shown as the satellite passes over a typhoon in the Philippine Sea (30°N), measuring wave heights of 9 m and wind speeds up to 20 m s^{-1}. As the track continues (40°N), it passes over the Kamtschatka Peninsula and finally enters open waters moving toward the Arctic Ocean. As shown in this figure, the quality-assurance algorithm successfully flags erroneous data while not discarding quality observations, even in areas where there are strong spatial gradients of wind speed and/or wave height.

Over the full duration of each satellite mission, the quality-control procedure removed inappropriate data records amounting to 15.5% for *Geosat*, 9.6% for *ERS-1*, 8.1% for *ERS-2*, 4.7% for TOPEX, 9.0% for *GFO*, 8.4% for *Jason-1*, and 17.1% for *Envisat*.

b. Altimeter calibration

Calibration of the altimeter data was carried out by comparing buoy measurements with quasi-simultaneous radar observations for both significant wave height H_s and wind speed U_{10}. In the case of altimeter wind speed, a single wind speed model relating wind speed to radar cross section σ_o applicable to all altimeter platforms was determined (see later in this section). Comparisons be-

tween buoy and satellite altimeter data require criteria for the spatial and temporal separation between such observations to be adopted. Following Dobson et al. (1987), Monaldo (1988), Gower (1996), Queffeulou (2003, 2004), and Queffeulou et al. (2004), these limits were set at 50 km and 30 min, respectively. Because buoy data were largely reported hourly (Hamilton 1986), the largest temporal separation is 30 min; following Monaldo (1988), such a time separation leads to an expected uncertainty of 0.5 m s^{-1} for wind speed and 0.3 m for significant wave height.

Along-track averages were calculated for all matching transects (maximum 100 km; i.e., ±50 km, assuming there is no land over the 100 km), and time tags of each altimeter overpass were linearly interpolated to the two nearest hourly buoy records for H_s and U_{10}, respectively. The 50-km spatial separation criterion defines a circle of diameter 100 km in which data are considered. A transect that passes directly over the buoy will have a transect length of 100 km. More distant passes will define shorter chords of the circle. Only transects with more than 4 valid points were considered to ensure statistically stable values. To ensure that the point buoy measurements and the spatially averaged altimeter data are comparable, it is desirable not to consider data recorded close to land, where there may be strong spatial gradients of wave height or wind speed. Therefore, buoy stations within 40 km of land were not considered in the calibration process (Dobson et al. 1987).

Dobson et al. (1987) and Monaldo (1988) analyzed typical errors associated with altimeter–buoy comparisons, considering spatial and temporal separation, buoy record duration, and altimeter footprint averaging size, as well as platform-specific instrumental error. Monaldo

(1988) concluded that differences for H_s and U_{10} of approximately 0.4 m and 1.8 m s^{-1}, respectively, can be expected when comparing altimeter and buoy estimates, whereas Dobson et al. (1987) determined that an overall rms uncertainty for H_s and U_{10} of 0.5 m and 1.8 m s^{-1}, respectively, may be expected using collocated measurements within a 50-km range.

Collocated buoy–altimeter measurements were compared using linear regression analysis. Because both variables (buoy and altimeter) have measurement uncertainty associated with them, a traditional regression analysis is not appropriate (Stoffelen 1998). Rather, a reduced major axis (RMA) regression was used to estimate the best fit between the two measurements (Trauth 2007). RMA regression is applicable when errors in both quantities need to be considered. The RMA methodology minimizes the triangular area between the data point and the regression line (Trauth 2007). Major outliers were eliminated prior to application of the RMA analysis. This was achieved by applying a robust regression algorithm and eliminating data points with low weighting. Robust regression is an iteratively reweighted least squares analysis (O'Leary 1990).

Figure 4 illustrates a typical calibration result for *Jason-1* altimeter data. Clearly observable is the significantly higher scatter for U_{10} than for H_s. Note that scatterplots for all other satellites look similar and therefore are not shown (resulting RMA analyses for all satellites are given in Table 3).

To evaluate the suitability of the final regression analysis, the following statistical parameters were evaluated: rmse [Eq. (2)], mean absolute error [MAE; Eq. (3)], Pearson's correlation coefficient ρ [Eq. (4)], the number of sample points, and the number of outliers.

$$\text{rmse: } \epsilon = \sqrt{\frac{1}{n}\sum_{i}^{n}(\hat{y}-y)^2}, \tag{2}$$

$$\text{MAE: } e = \frac{1}{n}\sum_{i}^{n}|\hat{y}-y|, \quad \text{and} \tag{3}$$

$$\rho(Y,\hat{Y}) = \frac{\text{Cov}(Y,\hat{Y})}{\sqrt{\text{Cov}(Y,Y)\text{Cov}(\hat{Y},\hat{Y})}}. \tag{4}$$

In Eqs. (2)–(4), the hat separates the estimate (calibrated value) from the reference measurement (buoy observation) and Cov is the covariance between two random variables. The values of y take on either H_s or U_{10}, and the uppercase values refer to vectors.

Although the RMA analysis can be performed directly for values of H_s, its application for U_{10} first requires the adoption of an appropriate wind speed algorithm relating U_{10} and the radar cross section σ_o. A wide range of such wind speed algorithms has been published. In general, one can distinguish between one- and two-parameter wind speed models (Fig. 5). Among others, Monaldo and Dobson (1989) and Gourrion et al. (2002, hereafter GO02) investigated the enhancement of wind speed estimates by adding significant wave height as an additional parameter in the wind speed function. A comprehensive summary of wind speed algorithms (including equations) can be found in Young (1993) and Young and Holland (1996). In this analysis, all major wind speed algorithms, including BR81, Chelton and McCabe (1985), CW86, GD85, WC91, and FC94, as well as the recent models from GO02 and A07, were compared with NODC buoy measurements and validated for performance using rms error estimates from Eq. (2). Published wind speed algorithms were typically derived for one particular altimeter platform (e.g., for *Seasat*, as in Chelton and McCabe 1985), thus the possibility of a platform-related bias (cf. Table 2) has to be considered before applying a uniform wind speed model to the data from multiple altimeter missions. With the present dataset, it would be possible to develop and fit an optimal functional form to the combined dataset of U_{10}–σ_o values. However, because the many existing functions are very similar, as shown in Fig. 5, such a process was not attempted. However, comparisons with available data showed that there were clear σ_o offsets between the datasets; when applying an algorithm to a satellite for which it was not derived, the offset needs to be considered. The rms error ϵ between the wind speed model and in situ buoy measurements was minimized by selecting the optimal offset for the radar cross section σ_o. The resulting values are shown in Table 2. These offset values need to first be applied before a specific algorithm can be applied to a specific satellite dataset. It is clear that the bulk of the available data in Fig. 5 is concentrated between 4 and 10 m s^{-1}. To ensure the algorithm fit is not biased to this region, data were averaged into 5 cm s^{-1} bins and these average values were used in the optimization.

It remains unclear if sea-state dependence, particularly significant wave height H_s, should be considered. Although this was the subject of previous research (e.g., Monaldo and Dobson 1989; Glazman and Greysukh 1993; GO02), results differ. As stated by Monaldo and Dobson (1989), significant wave height potentially affects the physical link between σ_o and surface wind speed in two ways. First, the local wave heights are the combination of waves that propagate into the area and wind waves generated by local wind fields. Second, the presence of waves may affect the development of short waves on the surface, which influence the radar cross section. Distinguishing such affects within the scatter of
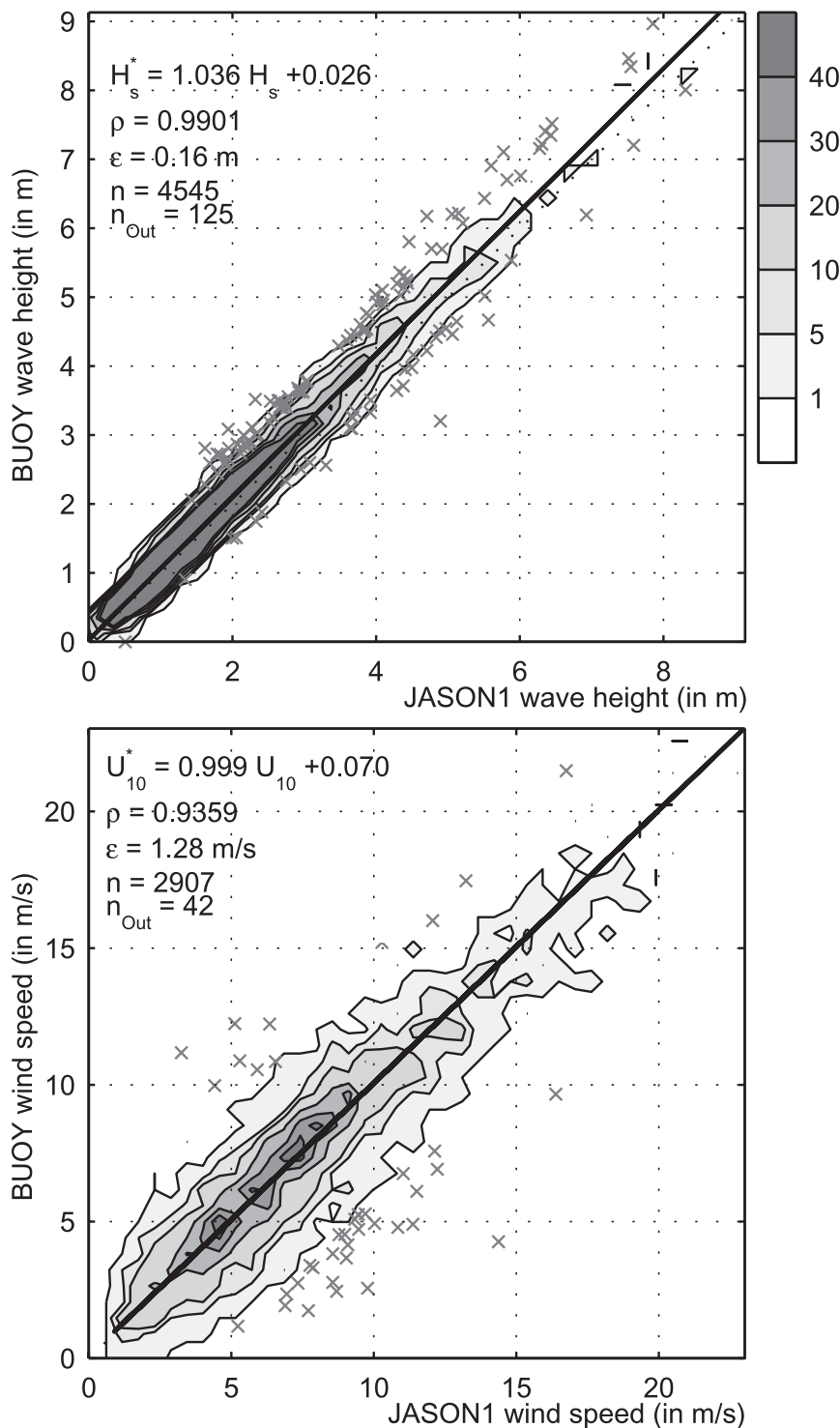
FIG. 4. Calibration results for *Jason-1* altimeter data. Shaded scatter density plots for (top) significant wave height and (bottom) wind speed of collocated measurements are shown. Collocated measurements are considered within 50-km radius and 30-min temporal separation. Error statistics for rmse ϵ, correlation coefficient ρ, and number n of sample points are given, with outliers n_{out} labeled with crosses. The solid line represents the RMA fit. The axes were divided into 40 even increments, and the contours show the number of data points in each increment square.
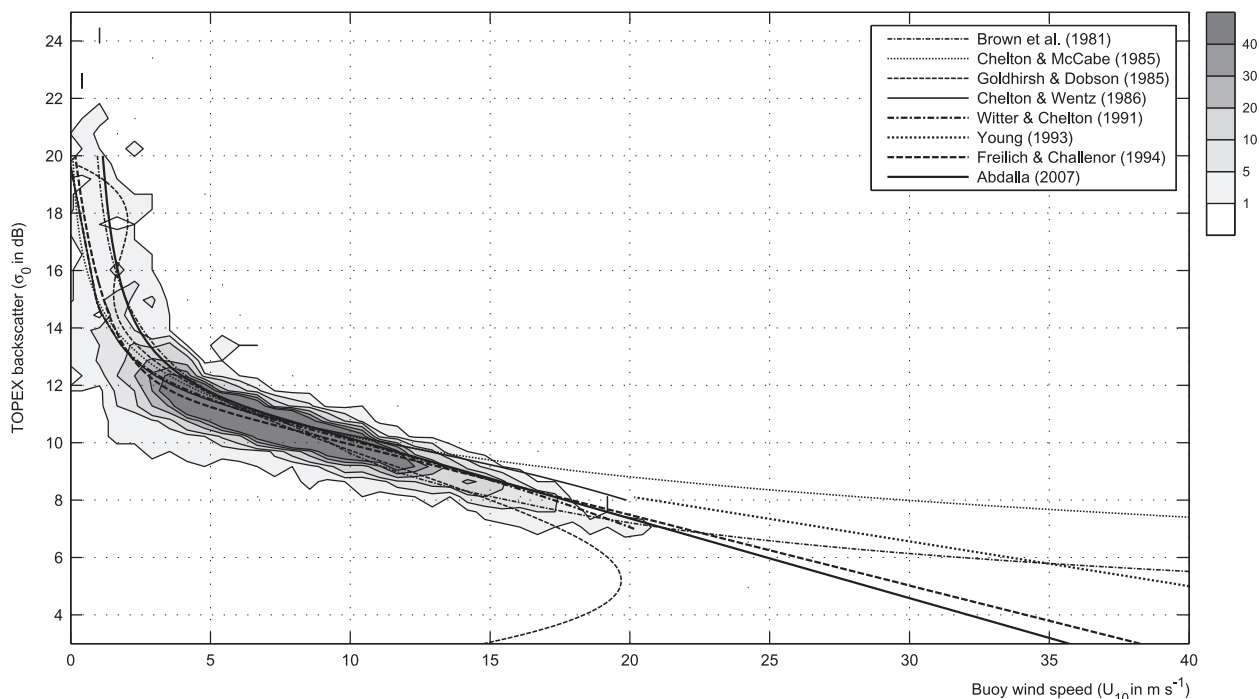
FIG. 5. Comparison of proposed wind speed algorithms for the estimation of wind speed U_{10} from the altimeter radar backscatter σ_o. The shaded contour plot shows isolines of data point density. The axes were each divided into 40 equally sized bins, and the number of data points in each bin was determined. Data are shown for TOPEX normalized radar cross section σ_o adjusted by -0.502 dB. Note that, with the exception of Young (1993), algorithms have been developed with data less than $U_{10} \approx 20$ m s^{-1}. The results have been extrapolated beyond this value to show the effect of extrapolation to such wind speeds.

the data is challenging, as seen in Fig. 5. The error analysis in Table 2 shows no clear reduction in rms error with the inclusion of H_s as an additional parameter. For these reasons, two-parameter functions involving H_s have not been considered further in this analysis.

Based on error statistics from Eqs. (2)–(4) the model proposed by A07 was selected as the default wind speed algorithm for the database and is briefly described later. A07 investigated the relationship between surface wind speed, as obtained from the numerical wind model of the European Centre for Medium-Range Weather Forecasting (ECMWF) and Ku-band altimeter backscatter coefficients from *Envisat*. The resulting algorithm was derived from two months (January–February 2005) of collocation data containing approximately 163 000 samples. Finally, the algorithm was verified against model wind speed for *Envisat* (2 yr), *Jason-1* (18 months), and *ERS-2* (5 yr) altimeter measurements. A07 adopted a two-branch approach to estimate a first-guess wind speed U_m by fitting linear and exponential segments for lower and higher radar cross section σ_o, respectively [cf. Eq. (5)]:

$$U_m = \begin{cases} 46.5 - 3.6\sigma_o & \text{for} \quad \sigma_o \leq 10.917 \text{ dB} \\ 1690 \exp(-0.5\sigma_o) & \text{for} \quad \sigma_o > 10.917 \text{ dB} \end{cases}.$$
$$(5)$$

Fine-tuning was carried out to ensure that model wind speeds matched buoy observations, with U_m from Eq. (5) adjusted to

$$U_{10} = U_m + 1.4U_m^{0.096} \exp(-0.32U_m^{0.096}). \quad (6)$$

In Eqs. (5) and (6), wind speed values have units of m s^{-1} and radar cross section has units of decibels. Since 24 October 2005, Eqs. (5) and (6) have been used operationally for the *Envisat* radar altimeter (A07).

As the A07 relationship was derived for data with $U_{10} < 18$ m s^{-1}, a modified form of the Young (1993) high wind speed relationship was adopted for $U_{10} > 18$ m s^{-1}. The offset in Eq. (7) was modified such that it intercepts the A07 result at 18 m s^{-1}:

$$U_{10} = -6.4\sigma_o + 69, \quad \text{if} \quad \text{Eq. (6)} > 18 \text{ m s}^{-1}. \quad (7)$$

In Eq. (7), U_{10} has units of meters per second and σ_o has units of decibels. Although the error statistics supported the adoption of the A07 algorithm as the preferred wind speed model, a visual inspection of Table 2 shows that the widely applied WC91 algorithm also performs well.

With an appropriate wind speed algorithm adopted, it is possible to carry out the calibrations of both H_s and

TABLE 2. Platform-specific σ_o bias (i.e., the reported bias needs to be added to the satellite σ_o values) with related rmse ϵ for selected wind speed algorithms: BR81, GD85, CW86, WC91, FC94, A07, and GO02. The column in boldface denotes the applied wind speed model.

Altimeter	BR81	GD85	CW86	WC91	FC94	A07	GO02
ERS-1	−0.205 dB	−0.264 dB	+0.095 dB	−0.039 dB	−0.177 dB	**+0.075 dB**	+0.578 dB
ϵ	1.32 m s^{-1}	1.23 m s^{-1}	1.41 m s^{-1}	1.20 m s^{-1}	1.26 m s^{-1}	**1.14 m s^{-1}**	1.18 m s^{-1}
ERS-2	−0.154 dB	−0.241 dB	+0.093 dB	−0.045 dB	−0.209 dB	**+0.075 dB**	+0.512 dB
ϵ	1.32 m s^{-1}	1.27 m s^{-1}	1.62 m s^{-1}	1.34 m s^{-1}	1.45 m s^{-1}	**1.25 m s^{-1}**	1.29 m s^{-1}
Envisat	−0.363 dB	−0.431 dB	−0.114 dB	−0.268 dB	−0.424 dB	**−0.138 dB**	+0.299 dB
ϵ	1.31 m s^{-1}	1.26 m s^{-1}	1.56 m s^{-1}	1.33 m s^{-1}	1.39 m s^{-1}	**1.21 m s^{-1}**	1.27 m s^{-1}
Geosat	−0.060 dB	−0.053 dB	+0.160 dB	+0.087 dB	−0.073 dB	**+0.225 dB**	+0.595 dB
ϵ	1.71 m s^{-1}	1.68 m s^{-1}	1.96 m s^{-1}	1.80 m s^{-1}	1.91 m s^{-1}	**1.75 m s^{-1}**	1.98 m s^{-1}
GFO	−0.731 dB	−0.796 dB	−0.433 dB	−0.595 dB	−0.755 dB	**−0.481 dB**	−0.031 dB
ϵ	1.37 m s^{-1}	1.32 m s^{-1}	1.64 m s^{-1}	1.39 m s^{-1}	1.47 m s^{-1}	**1.28 m s^{-1}**	1.36 m s^{-1}
Jason-1	−1.036 dB	−1.115 dB	−0.779 dB	−0.939 dB	−1.056 dB	**−0.789 dB**	−0.361 dB
ϵ	1.38 m s^{-1}	1.36 m s^{-1}	1.72 m s^{-1}	1.44 m s^{-1}	1.54 m s^{-1}	**1.33 m s^{-1}**	1.36 m s^{-1}
TOPEX	−0.752 dB	−0.837 dB	−0.469 dB	−0.627 dB	−0.777 dB	**−0.502 dB**	−0.108 dB
ϵ	1.27 m s^{-1}	1.21 m s^{-1}	1.49 m s^{-1}	1.21 m s^{-1}	1.32 m s^{-1}	**1.14 m s^{-1}**	1.16 m s^{-1}

U_{10} for each of the altimeters. Table 3 provides the RMA-derived calibration results for each of the satellites. The results shown represent the average over the entire period of operation for each satellite mission and utilize all collocated buoy observations over that period. In addition, a subset of published altimeter calibration models is also shown for comparison purposes.

Queffeulou (2003) adopted a very similar calibration approach (averaging altimeter transect within 50-km radius and 30-min temporal separation) to that proposed here, but it was based on a shorter database. As can be seen from Table 3, the present results are in good agreement with Queffeulou (2003) for H_s across all satellite missions. Young (1999a) used a database of 10-yr duration but compared monthly means within $4° \times 4°$ bins rather than collocated passes. This different methodology appears to give rise to measurable differences in the calibration results.

For *Geosat* H_s, Dobson et al. (1987) proposed that the altimeter is generally 0.40 m lower than buoy observations ($\epsilon = 0.49$ m, $e = 0.36$ m, and $n = 116$). Carter et al. (1992) provided evidence for a *Geosat* scaling error with altimeter values being 13% lower than buoy values. However, ordinary least squares regression, not forced through the origin, leads to $H_s^* = 1.093\,H_s + 0.116$ ($n = 164$), where H_s^* is the corrected significant wave height (Carter et al. 1992), which is in good agreement with the result presented here.

Ray and Beckley (2003) correlated TOPEX and *Jason-1* significant wave height with buoy observations and concluded that $H_s^* = 1.046 H_s − 0.070$ ($\epsilon = 0.17$ m, $\rho = 0.985$, and $n = 399$) for TOPEX and $H_s^* = 1.100\,H_s − 0.104$ ($\epsilon = 0.21$ m, $\rho = 0.983$, and $n = 368$) for *Jason-1*. The TOPEX result is in excellent agreement with the present result, which uses approximately 10 times the

amount of data. The *Jason-1* result differs slightly from the present result, with a larger slope but more negative offset.

For wind speed, it is not possible to directly compare the results with previous calibrations. In the present analysis, the A07 wind speed algorithm was adopted for all satellites, but with a σ_o offset for each satellite chosen to reduce the rms error. The resulting values of altimeter wind speed were then further calibrated against collocated buoy wind speed using the RMA analysis. Not surprisingly, the results all have regression slopes near 1.00 and small offsets.

c. Altimeter collocation analysis

For much of the period under consideration (since 1993), multiple altimeter missions have been in orbit. As a result, it is possible to cross-validate instrument performance against other platforms by comparing observations at crossover points. Ground-track crossovers between simultaneously operating altimeter platforms were considered when both platforms passed the same ground point within 30 min. In contrast to Queffeulou (2004), 100-km (50 km each side) along-track averages were compared, rather than the closest 1-s measurements. As for the buoy comparisons, the spatial average provides a more statistically stable comparison than a single-point observation. For all platforms, a valid ground track contains at least 10 individual 1-s altimeter data points for averaging. The altimeter crossover analysis was not used to calibrate individual platforms; this process is undertaken with the buoy analysis (cf. section 3b). Rather, scatterplots comparing different altimeters at crossover points were used for independent validation of the calibrated results. In other words, the crossover analysis was used as a quality-control and validation measure.

TABLE 3. Overall calibration results using RMA regression. The analysis uses all available buoy–altimeter collocations n for the full period of each altimeter mission. Also shown are results from earlier studies. Altimeter wind speed U_{10} was calculated from the A07 model and platform-specific biases were applied (cf. Table 2).

		Zieger, Vinoth and Young (2009)						Queffeulou et al. (2004) for H_s / Queffeulou (2003) for U_{10}				Young (1999a)		
	Altimeter	Slope	Offset	ϵ	e	ρ	n	Slope	Offset	ϵ	n	Slope	Offset	n
H_s	Envisat	1.069	−0.198	0.15 m	0.12 m	0.990	4390	1.033	−0.183	0.19 m	1280			
	ERS-1	1.127	+0.280	0.20 m	0.16 m	0.984	2079					1.243	+0.040	192
	ERS-2	1.076	+0.042	0.17 m	0.13 m	0.989	7885	1.064	+0.001	0.19 m	12 070			
	Geosat	1.076	+0.122	0.21 m	0.17 m	0.982	1600					1.144	−0.148	203
	GFO	1.068	+0.102	0.15 m	0.12 m	0.991	6179	1.080	+0.039		21 228			
	Jason-1	1.036	+0.026	0.16 m	0.13 m	0.990	4420	1.007	+0.039	0.19 m	2853			
	TOPEX	1.049	−0.098	0.17 m	0.13 m	0.990	3428	1.024	−0.048	0.17 m	7826	1.067	−0.079	192
U_{10} (A07)	Envisat	1.010	−0.110	1.11 m s^{-1}	0.86 m s^{-1}	0.941	2926	0.964	+0.599	1.52 m s^{-1}	292			
	ERS-1	1.047	−0.293	1.07 m s^{-1}	0.83 m s^{-1}	0.984	1333					0.849	+1.217	192
	ERS-2	1.005	−0.024	1.20 m s^{-1}	0.93 m s^{-1}	0.931	5093							
	Geosat	1.015	−0.087	1.76 m s^{-1}	1.31 m s^{-1}	0.857	1113					0.874	+0.337	196
	GFO	0.986	−0.059	1.31 m s^{-1}	1.02 m s^{-1}	0.925	4136							
	Jason-1	0.999	+0.070	1.28 m s^{-1}	0.99 m s^{-1}	0.936	2865	0.986	+0.887	0.85 m s^{-1}	1236			
	TOPEX	1.010	−0.062	1.11 m s^{-1}	0.87 m s^{-1}	0.948	2486					0.943	+1.847	190

Figure 6 shows an example of the spatial coverage of crossover points for the overlap period of *Jason-1* and *ERS-2*. In comparison to the buoy calibration process, the very much larger number of collocations is clear. Figure 7 shows the resulting wave height and wind speed scatterplots for this same case. For all combinations of coincident satellite missions, the calibrated satellite altimeters produced consistent results (RMA regression slope close to 1:1), when averaged over the full durations of coincident operation.

d. Long-term monitoring

The calibrations performed against buoy data (Table 3) considered all available data for the period of operation of each satellite. As a result, the calibrations are averages over the full satellite missions. It is important to

FIG. 6. Distribution of collocated measurements between *Jason-1* and *ERS-2* radar altimeters. During the latter part of the *ERS-2* mission, an onboard storage failure limited the spatial coverage to the Northern Hemisphere. As a result, there is a greater density of collocation points in the North Atlantic and parts of the North Pacific.

ensure that the calibrations do not vary over the duration of the extended mission. This could be determined by examining differences between buoy and altimeter data as a function of time. A further possibility is to examine differences between coincident altimeter missions as a function of time at crossover points. Because of the very much larger datasets for altimeter crossover points, this second option proved more reliable, with a greater capability in identifying small changes in instrument performance.

Figure 8 shows an example of the differences between TOPEX and *ERS-2* values of H_s. Because of the large number of observations, data points shown in the plot were thinned using block averages over n points (values of n are given in figure captions; e.g., 20/1 for a 20-point blocked average). If significant discontinuities or data drifts were determined, the datasets were partitioned and a reduced major axis regression was applied for each section of mission. For consistency, the partitioned RMA regression was performed against buoy data, with the crossover analysis acting as an independent quality control. For wind speed measurements, the previously determined satellite-specific σ_o offsets were retained, and any further departures from buoy measurements are corrected using the partitioned RMA analysis. Once the partitioned RMA analysis had been applied, the satellite crossover plots were examined to ensure the process had removed any inconsistencies between the datasets.

The most obvious example of a time-specific variation in altimeter performance is the TOPEX drift in H_s, which commenced at approximately cycles 163–170 and continues to cycle 235 (April 1997–January 1999),
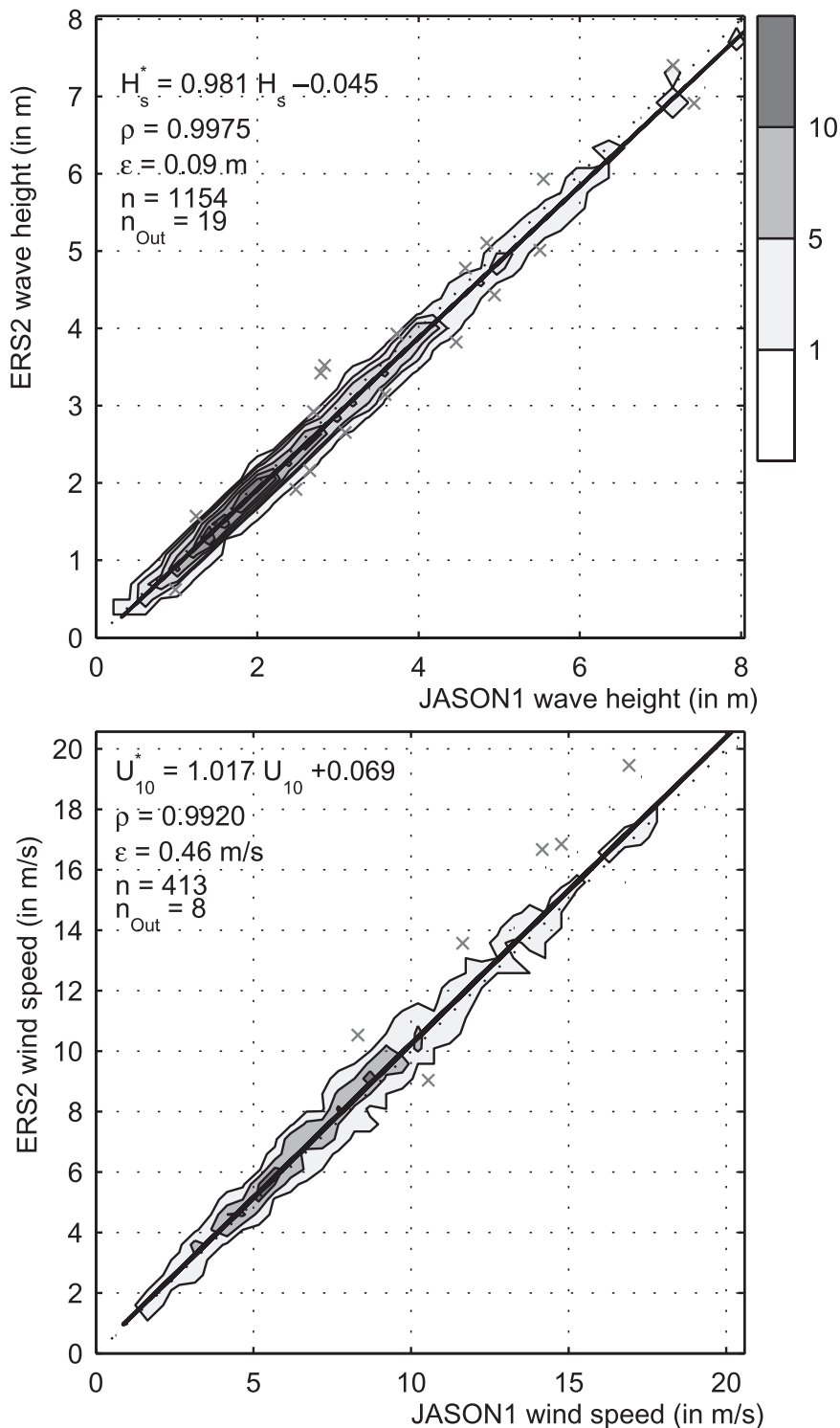
FIG. 7. Collocated measurements between *Jason-1* and *ERS-2* altimeters. Shaded scatter density plots show (top) significant wave height and (bottom) wind speed. Contours are calculated as in Fig. 4.
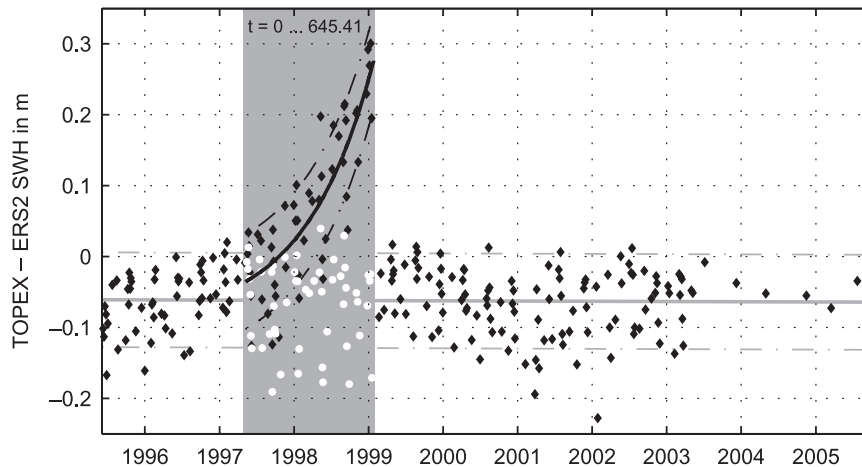
FIG. 8. Plot (20/1 block averages) illustrating differences in significant wave height between uncalibrated TOPEX and calibrated *ERS-2* measurements. The proposed drift correction *f(t)* [Eq. (8)] with *t* in days was applied between 25 Apr 1997 and 30 Jan 1999, equivalent to cycles 170 to 235. Dashed–dotted lines represent ½ std dev boundaries. The time period of the drift is shown by the shaded region. The white dots in this region shows the altimeter differences once the TOPEX drift has been removed using Eq. (8).

previously investigated by Challenor and Cotton (1999) and Queffeulou (2004). Challenor and Cotton (1999) applied a linear trend model to buoy measurements to remove the drift, whereas Queffeulou (2004) fitted a third-order polynomial using *ERS-2* as the reference dataset. As illustrated in Fig. 8, the drift can be well approximated by an exponential power function of the form

$$f(t) = 0.0542[\exp(0.0027t)]^{1.1080} - 0.0303, \qquad (8)$$

where the dependent variable t is time, measured in days from 25 April 1997, and $f(t)$ has units of meters. The correction is valid until 30 January 1999 (0 days $\leq t <$ 645 days). Figure 8 also shows the results once TOPEX data have been corrected using Eq. (8).

Figure 9 shows the difference between TOPEX and buoy H_s after the removal of the drift. In both cases, Eq. (8) successfully corrects the data. The reduction in available data in Fig. 8 since June 2003 is a result of an onboard storage failure on *ERS-2*, which has limited
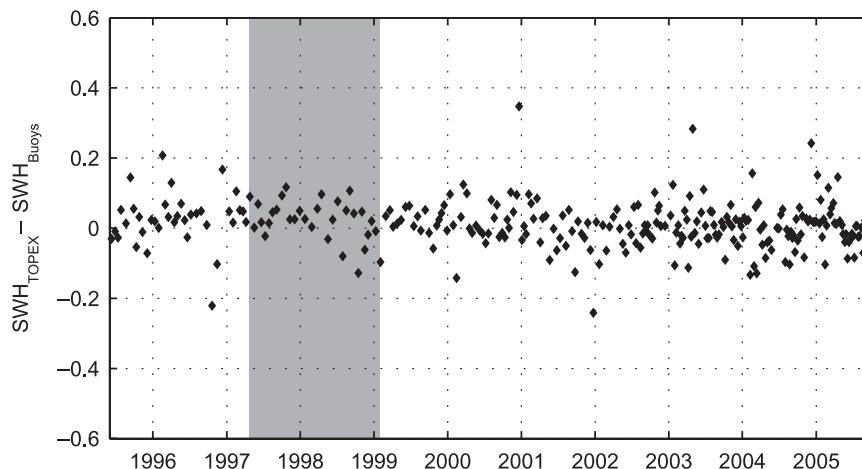

FIG. 9. Differences in H_s between TOPEX and buoy observations after applying drift correction [Eq. (8)] and calibration function (cf. Table 4). The plot (block averaged at 12/1) covers the same time span as in Fig. 8.
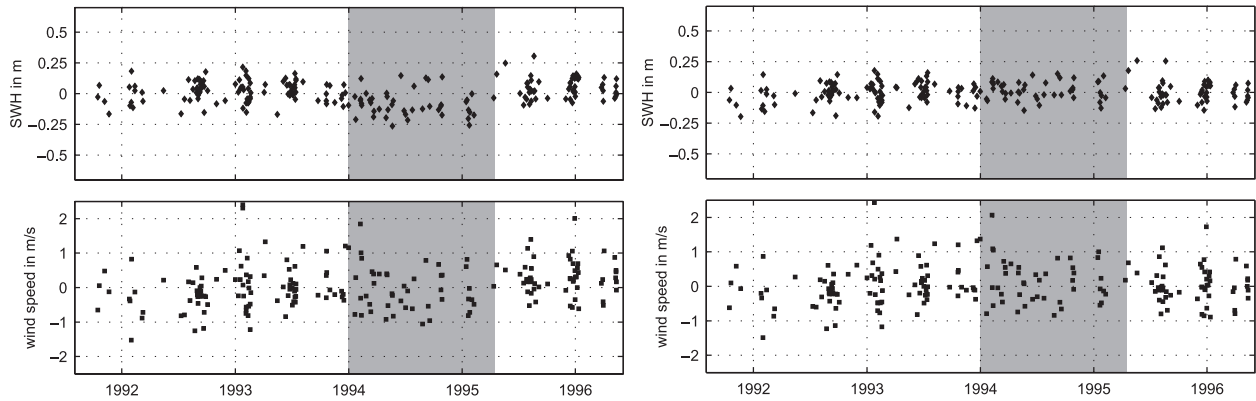
FIG. 10. (left) Plot (block averaged at 12/1) showing differences between *ERS-1* and buoy H_s and U_{10}. The shaded region shows a time-dependent offset in H_s. (right) The differences once the partial RMA analysis was performed, removing the offset, are shown. Error statistics prior to the partial RMA analysis are $\epsilon_{H_s} = 0.20\,\mathrm{m}, \epsilon_{U_{10}} = 1.11\,\mathrm{m\,s^{-1}}$. The partial RMA analysis reduces these values to $\epsilon_{H_s} = 0.19\,\mathrm{m}$ and $\epsilon_{U_{10}} = 1.10\,\mathrm{m\,s^{-1}}$.

available data from this satellite to locations in the Northern Hemisphere close to receiving stations. This feature is also apparent in Fig. 6.

Changes in altimeter calibration for either U_{10} or H_s were identified for *ERS-1*, *ERS-2*, *GFO*, and TOPEX using this process. Figure 10 shows differences between buoy and *ERS-1* H_s and U_{10} for the duration of the *ERS-1* mission. As previously explained, changes to calibration were actually identified using altimeter crossover comparisons. The partial recalibration was then performed against buoy data and checked using crossover comparisons. Because no single pair of altimeters covers the full *ERS-1* mission, the buoy comparison is used here for illustrative purposes. The period between 1 January 1994 and 18 February 1995 clearly shows slightly low values of H_s. To correct this effect, the full *ERS-1* mission was divided into three sections and the partial RMA analysis was applied to each section.

Figure 10 (right) shows the corrected results, with the offset removed.

Figure 11 shows a similar plot for *GFO*. Here, discontinuities in U_{10} in the periods before 21 December 2000 and after 21 January 2007 are clear. Again, the partial RMA analysis successfully accounted for these anomalies.

The source of these inconsistencies is unclear and may result from changes to onboard systems, different software implementations, etc. Although the long-term differences are relatively small (generally less than 1 m s^{-1} in wind speed and 0.2 m in wave height), the value of a long-term database of this type requires confidence in the long-term stability of the data.

In the case of TOPEX, the altimeter was changed from the Side A instrument to Side B in February 1999. The data did not show a measurable discontinuity at this point or any clear degradation in the quality of the Side A data leading up to the change. This result is consistent
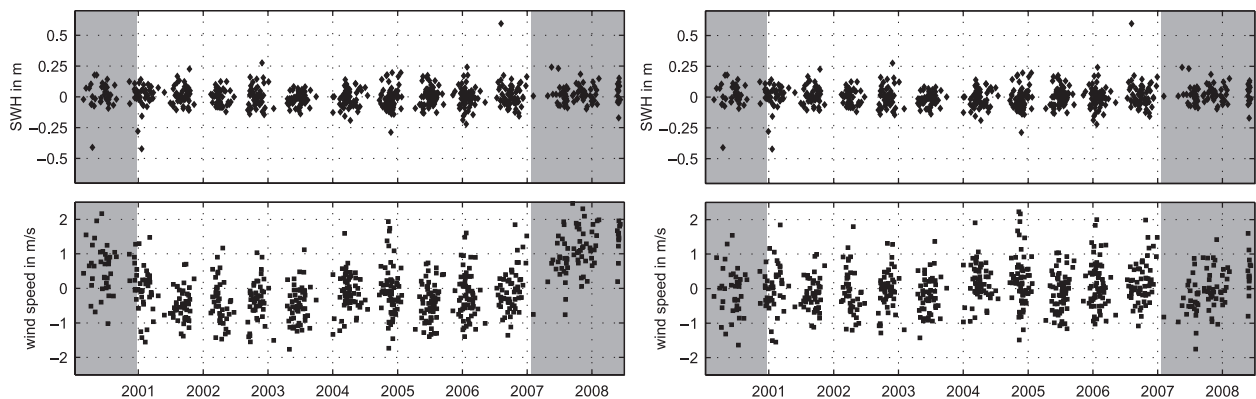

FIG. 11. Differences between *GFO* and buoy H_s and U_{10}. Deviations (shaded areas) in *GFO* wind speed measurements were successfully removed using the partial RMA calibration approach. Wind speed rmse was improved from (left) $\epsilon_{U_{10}} = 1.20\,\mathrm{m\,s^{-1}}$ to (right) $\epsilon_{U_{10}} = 1.18\,\mathrm{m\,s^{-1}}$, whereas significant wave height was not altered: $\epsilon_{H_s} = 0.15\,\mathrm{m}$.

TABLE 4. Calibration results for all altimeters and periods over which the calibration is valid. Results are shown for both significant wave height H_s and 10-m wind speed U_{10}, where the asterisk indicates the corrected value. Error statistics, rmse ϵ, mean absolute error e, correlation coefficient ρ, the number of samples n, rate of outliers, and the number of buoy stations used for the calibrations are shown.

	Altimeter	Scope	Calibration function	ϵ	e	ρ	n	Outlier	Buoys
H_s	Envisat	24 Sep 2002–17 Nov 2008	$H_s^* = 1.069 \cdot H_s - 0.201$	0.156 m	0.118 m	0.990	4506	2.6%	87
	ERS-1	1 Aug 1991–1 Jan 1994	$H_s^* = 1.122 \cdot H_s + 0.255$	0.193 m	0.148 m	0.985	1005	1.7%	58
	ERS-1	1 Jan 1994–18 Apr 1995	$H_s^* = 1.150 \cdot H_s + 0.366$	0.215 m	0.169 m	0.986	510	1.0%	58
	ERS-1	18 Apr 1995–2 Jun 1996	$H_s^* = 1.102 \cdot H_s + 0.273$	0.177 m	0.135 m	0.988	595	2.2%	58
	ERS-2	29 Apr 1995–8 Sep 2008	$H_s^* = 1.076 \cdot H_s + 0.042$	0.172 m	0.132 m	0.989	8060	2.2%	87
	Geosat	31 Mar 1985–30 Dec 1989	$H_s^* = 1.076 \cdot H_s + 0.122$	0.216 m	0.166 m	0.982	1638	2.3%	42
	GFO	7 Jan 2000–1 Jul 2008	$H_s^* = 1.068 \cdot H_s + 0.102$	0.155 m	0.117 m	0.991	6252	2.9%	78
	Jason-1	15 Jan 2002–3 May 2008	$H_s^* = 1.036 \cdot H_s + 0.026$	0.164 m	0.125 m	0.990	4545	2.8%	60
	TOPEX	25 Sep 1992–8 Oct 2005	$H_s^* = 1.050 \cdot H_s - 0.088$	0.162 m	0.124 m	0.991	3510	2.5%	45
U_{10} (A07)	Envisat	24 Sep 2002–17 Nov 2008	$U_{10}^* = 1.010 \cdot U_{10} - 0.110$	1.097 m s^{-1}	0.860 m s^{-1}	0.941	2979	1.8%	87
	ERS-1	1 Aug 1991–1 Jan 1994	$U_{10}^* = 1.066 \cdot U_{10} - 0.395$	1.056 m s^{-1}	0.827 m s^{-1}	0.944	653	1.7%	58
	ERS-1	1 Jan 1994–18 Apr 1995	$U_{10}^* = 1.025 \cdot U_{10} + 0.128$	1.056 m s^{-1}	0.800 m s^{-1}	0.946	328	2.1%	58
	ERS-1	18 Apr 1995–2 Jun 1996	$U_{10}^* = 1.046 \cdot U_{10} - 0.562$	1.040 m s^{-1}	0.807 m s^{-1}	0.952	377	1.3%	58
	ERS-2	29 Apr 1995–12 Feb 2000	$U_{10}^* = 1.043 \cdot U_{10} - 0.071$	1.114 m s^{-1}	0.862 m s^{-1}	0.939	1693	2.1%	87
	ERS-2	12 Feb 2000–10 Feb 2001	$U_{10}^* = 0.980 \cdot U_{10} - 0.119$	1.102 m s^{-1}	0.884 m s^{-1}	0.936	331	0.0%	87
	ERS-2	10 Feb 2001–24 May 2005	$U_{10}^* = 0.972 \cdot U_{10} - 0.036$	1.162 m s^{-1}	0.914 m s^{-1}	0.934	1832	1.7%	87
	ERS-2	24 May 2005–8 Sep 2008	$U_{10}^* = 1.041 \cdot U_{10} - 0.101$	1.214 m s^{-1}	0.959 m s^{-1}	0.931	1312	1.2%	87
	Geosat	31 Apr 1985–30 Dec 1989	$U_{10}^* = 1.015 \cdot U_{10} - 0.087$	1.706 m s^{-1}	1.306 m s^{-1}	0.857	1166	4.5%	42
	GFO	7 Jan–21 Dec 2000	$U_{10}^* = 0.976 \cdot U_{10} - 0.623$	1.234 m s^{-1}	0.962 m s^{-1}	0.915	340	1.2%	78
	GFO	21 Dec 2000–21 Jan 2007	$U_{10}^* = 1.015 \cdot U_{10} + 0.033$	1.099 m s^{-1}	0.853 m s^{-1}	0.949	3283	2.1%	78
	GFO	21 Jan 2007–1 Jul 2008	$U_{10}^* = 0.903 \cdot U_{10} - 0.489$	1.179 m s^{-1}	0.930 m s^{-1}	0.929	491	1.6%	78
	Jason-1	15 Jan 2002–3 May 2008	$U_{10}^* = 0.999 \cdot U_{10} + 0.070$	1.280 m s^{-1}	0.993 m s^{-1}	0.936	2907	1.4%	60
	TOPEX	22 Sep 1992–10 Feb 2001	$U_{10}^* = 0.991 \cdot U_{10} + 0.003$	1.079 m s^{-1}	0.851 m s^{-1}	0.945	1243	1.7%	45
	TOPEX	10 Feb 2001–21 Oct 2003	$U_{10}^* = 1.031 \cdot U_{10} - 0.140$	1.097 m s^{-1}	0.857 m s^{-1}	0.953	662	1.5%	45
	TOPEX	21 Oct 2003–8 Oct 2005	$U_{10}^* = 1.018 \cdot U_{10} - 0.050$	1.130 m s^{-1}	0.877 m s^{-1}	0.949	620	1.6%	45

with the Side B calibration study reported by Dorandeu (1999).

The final calibrations for all satellites are provided in Table 4. Table 4 details the calibration results applicable in various periods for each satellite, as well as error statistics.

4. Conclusions

The data and procedures outlined here present a detailed analysis of the historic altimeter database of H_s and U_{10} over the more than two decades for which data are available. The process developed calibrates the altimeter records against buoy data and then independently validates these results against independent altimeter missions at crossover points of ground tracks. The value of such a dataset is in that it covers an extremely long duration with global coverage. As such, it is critical that the altimeter calibration is stable over this extended duration. This analysis investigates the long-term stability of the altimeter missions and concludes that the long-term drift of results is generally not an issue (with the exception of TOPEX H_s). However, a number of the missions exhibit apparent step changes in calibration at various times. Although these changes are not large, they do impact the overall quality and reliability of the dataset. However, these changes in calibration can be corrected by partitioning the datasets with time and independently calibrating the altimeter in each partitioned segment. The reason for these step changes in calibration does not appear to have been well documented and is presumably the result of changes in the software–hardware of the satellite or of processing methods.

A number of relations between the radar cross section and wind speed were investigated, and the A07 relationship was ultimately adopted for use with all altimeters. However, the analysis clearly shows that, before applying such a relationship across all altimeters, a platform-dependent offset must be applied.

Consistent with previous studies, altimeter values of H_s exhibit greater accuracy than U_{10}. Following calibration, the accuracies of the various altimeters are similar, with the rms error being less than 0.25 m for H_s and 1.7 m s^{-1} for U_{10}.

In this study, no attempt has been made to look at long-term trends in the final "calibrated" dataset. This is an involved task that requires a careful analysis of the data. However, the present dataset does provide a unique resource for such studies, and this is the subject of ongoing research.

REFERENCES

Abdalla, S., 2007: Ku-band radar altimeter surface wind speed algorithm. *Proc. Envisat Symp. 2007,* Montreux, Switzerland, European Centre for Medium-Range Weather Forecasts. [Available online at http://envisat.esa.int/envisatsymposium/proceedings/sessions/3E4/463250sa.pdf.]

Alves, J. H. G. M., and I. R. Young, 2003: On estimating extreme wave heights using combined Geosat, Topex/Poseidon and ERS-1 altimeter data. *Appl. Ocean Res.,* **25,** 167–186, doi:10.1016/j.apor.2004.01.002.

Bendat, J. S., and A. G. Piersol, 1971: *Random Data: Analysis & Measurement Procedures*. Wiley-Interscience, 407 pp.

Brown, G., H. Stanley, and N. Roy, 1981: The wind-speed measurement capability of spaceborne radar altimeters. *IEEE J. Oceanic Eng.,* **6,** 59–63.

Caires, S., A. Sterl, J. R. Bidlot, N. Graham, and V. Swail, 2004: Intercomparison of different wind–wave reanalyses. *J. Climate,* **17,** 1893–1913.

Callahan, P. S., C. S. Morris, and S. V. Hsiao, 1994: Comparison of TOPEX/POSEIDON σ_0 and significant wave height distributions to Geosat. *J. Geophys. Res.,* **99,** 25 015–25 024.

Carter, D. J. T., P. G. Challenor, and M. A. Srokosz, 1992: An assessment of Geosat wave height and wind speed measurements. *J. Geophys. Res.,* **97,** 11 383–11 392.

Challenor, P. G., and D. Cotton, 1999: Trends in TOPEX significant wave height measurement. Southampton Oceanography Centre Rep., 6 pp.

Chelton, D. B., and P. J. McCabe, 1985: A review of satellite altimeter measurement of sea surface wind speed: With a proposed new algorithm. *J. Geophys. Res.,* **90,** 4707–4720.

——, and F. J. Wentz, 1986: Further development of an improved altimeter wind speed algorithm. *J. Geophys. Res.,* **91,** 14 250–14 260.

——, J. C. Ries, B. J. Haines, L.-L. Fu, and P. S. Callahan, 2001: Satellite altimetry. *Satellite Altimetry and Earth Sciences: A Handbook of Techniques and Applications,* L.-L. Fu and A. Cazenave, Eds., Academic Press, 1–131.

Cheney, R. E., B. C. Douglas, R. W. Agreen, L. Miller, D. L. Porter, and N. Doyle, 1987: GEOSAT altimeter geophysical data record: User handbook. NOAA, 31 pp.

Cotton, P. D., and D. J. T. Carter, 1994: Cross calibration of TOPEX, ERS-1, and Geosat wave heights. *J. Geophys. Res.,* **99,** 25 025–25 033.

Dobson, E., F. Monaldo, J. Goldhirsh, and J. Wilkerson, 1987: Validation of Geosat altimeter-derived wind speeds and significant wave heights using buoy data. *J. Geophys. Res.,* **92,** 10 719–10 731.

Donelan, M. A., 1990: Air-sea interaction. *The Sea: Ocean Engineering Science,* John Wiley & Sons, 239–292.

Dorandeu, J., 1999: Side-B TOPEX altimeter evaluation. CLS/DOS/NT Rep. 99.175. [Available online at http://www-aviso.cnes.fr:8090/HTML/information/missions/topex/topex_b_uk.html.]

Evans, D., C. L. Conrad, and F. M. Paul, 2003: Handbook of automated data quality control checks and procedures of the National Data Buoy Center. NOAA National Data Buoy Center Tech. Document 03–02, 44 pp.

Freilich, M. H., and P. G. Challenor, 1994: A new approach for determining fully empirical altimeter wind speed model functions. *J. Geophys. Res.,* **99,** 25 051–25 062.

Glazman, R. E., and A. Greysukh, 1993: Satellite altimeter measurements of surface wind. *J. Geophys. Res.,* **98,** 2475–2483.

Goldhirsh, J., and E. Dobson, 1985: A recommended algorithm for the determination of ocean surface wind speed using a satellite-borne radar altimeter. Johns Hopkins University Applied Physics Laboratory Rep. JHU/APL SIR-85-U005.

Gourrion, J., D. Vandemark, S. Bailey, B. Chapron, G. P. Gommenginger, P. G. Challenor, and M. A. Srokosz, 2002: A two-parameter wind speed algorithm for Ku-band altimeters. *J. Atmos. Oceanic Technol.,* **19,** 2030–2048.

Gower, J. F. R., 1996: Intercalibration of wave and wind data from TOPEX/POSEIDON and moored buoys off the west coast of Canada. *J. Geophys. Res.,* **101,** 3817–3829.

Hamilton, G. D., 1986: National Data Buoy Center programs. *Bull. Amer. Meteor. Soc.,* **67,** 411–415.

Holthuijsen, L. H., 2007: *Waves in Oceanic and Coastal Waters*. Cambridge University Press, 387 pp.

Kshatriya, J., A. Sarkar, and R. Kumar, 2001: Comparison of TOPEX/POSEIDON altimeter derived wind speed and wave parameters with ocean buoy data in the north Indian Ocean. *Mar. Geod.,* **24,** 131–138.

Meindl, E. A., and G. D. Hamilton, 1992: Programs of the National Data Buoy Center. *Bull. Amer. Meteor. Soc.,* **73,** 985–993.

Monaldo, F., 1988: Expected differences between buoy and radar altimeter estimates of wind speed and significant wave height and their implications on buoy-altimeter comparisons. *J. Geophys. Res.,* **93,** 2285–2302.

——, and E. Dobson, 1989: On using significant wave height and radar cross section to improve radar altimeter measurements of wind speed. *J. Geophys. Res.,* **94,** 12 699–12 701.

NDBC, cited 2008: What are the sensors' reporting, sampling, and accuracy readings? NOAA/National Data Buoy Center. [Available online at http://www.ndbc.noaa.gov/rsa.shtml.]

NODC, cited 2008: File format description for meteorology, oceanography, and wave spectra data from buoys (National Oceanographic Data Center F291 format). NOAA/National Oceanographic Data Center. [Available online at http://www.nodc.noaa.gov/General/NODC-Archive/f291.html.]

O'Leary, D. P., 1990: Robust regression computation using iteratively reweighted least squares. *SIAM J. Matrix Anal. Appl.,* **11,** 466–480, doi:10.1137/0611032.

Queffeulou, P., 2003: Validation of ENVISAT RA-2 and JASON-1 altimeter wind and wave measurements. *Proc. IEEE Geosci. Remote Sens. Symp.,* **5,** 2987–2989, doi:10.1109/IGARSS.2003.1294656.

——, 2004: Long-term validation of wave height measurements from altimeters. *Mar. Geod.,* **27,** 495–510, doi:10.1080/01490410490883478.

——, A. Bentamy, and J. Guyader, 2004: Satellite wave height validation over the Mediterranean Sea. *Proc. Envisat & ERS Symp.,* Salzburg, Austria, European Space Agency, 208.1.

Ray, R. D., and B. D. Beckley, 2003: Simultaneous ocean wave measurements by the Jason and Topex satellites, with buoy and model comparisons. *Mar. Geod.,* **26,** 367–382, doi:10.1080/714044527.

Stoffelen, A., 1998: Toward the true near-surface wind speed: Error modeling and calibration using triple collocation. *J. Geophys. Res.,* **103,** 7755–7766.

Tolman, H. L., 2002: Validation of WAVEWATCH III version 1.15 for a global domain. OMB Tech. Note 213, 37 pp.

Trauth, M. H., 2007: *MATLAB Recipes for Earth Sciences*. 2nd ed. Springer Verlag, 288 pp.

Walker, D. M., 1995: Measurement techniques and capabilities of the Geosat Follow-On (GFO) radar altimeter. *Proc. Second Topical Symp. on Combined Optical-Microwave Earth and Atmosphere Sensing,* Atlanta, GA, IEEE, 226–228, doi:10.1109/COMEAS.1995.472314.

Witter, D. L., and D. B. Chelton, 1991: A Geosat altimeter wind speed algorithm and a method for altimeter wind speed algorithm development. *J. Geophys. Res.,* **96,** 8853–8860.

Young, I. R., 1993: An estimate of the Geosat altimeter wind speed algorithm at high wind speeds. *J. Geophys. Res.,* **98,** 20 275–20 285.

——, 1999a: An intercomparison of GEOSAT, TOPEX and ERS1 measurements of wind speed and wave height. *Ocean Eng.,* **26,** 67–81, doi:10.1016/S0029-8018(97)10016-6.

——, 1999b: *Wind-Generated Ocean Waves*. Elsevier Ocean Engineering Series, Vol. 2, Elsevier Science, 306 pp.

——, and G. J. Holland, 1996: *Atlas of the Oceans: Wind and Wave Climate*. Pergamon, 241 pp.